Available online at www.sciencedirect.com

SciVerse ScienceDirect

Proceedings of the Combustion Institute 34 (2013) 887–894

Proceedings of the Combustion Institute

www.elsevier.com/locate/proci

Modeled quenching limits of spherical hydrogen diffusion flames

V.R. Lecoustre [a], P.B. Sunderland [a,*], B.H. Chao [b], R.L. Axelbaum [c]

[a] Dept. of Fire Protection Engineering, University of Maryland, College Park, MD 20742, USA
[b] Dept. of Mechanical Engineering, University of Hawaii, Honolulu, HI 96822, USA
[c] Dept. of Energy, Environmental and Chemical Engineering, Washington University, St. Louis, MO 63130, USA

Available online 9 August 2012

Abstract

Hydrogen–air diffusion flames were modeled with an emphasis on kinetic extinction. The flames were one-dimensional spherical laminar diffusion flames supported by adiabatic porous burners of various diameters. Behavior of normal (H_2 flowing into quiescent air) and inverse (air flowing into quiescent H_2) configurations were considered using detailed H_2/O_2 chemistry and transport properties with updated light component diffusivities. For the same heat release rate, inverse flames were found to be smaller and 290 K hotter than normal flames. The weakest normal flame that could be achieved before quenching has an overall heat release rate of 0.25 W, compared to 1.4 W for the weakest inverse flame. There is extensive leakage of the ambient reactant for both normal and inverse flames near extinction, which results in a premixed flame regime for diffusion flames except for the smallest burners with radii on the order of 1 μm. At high flow rates $H + OH(+M) \rightarrow H_2O(+M)$ contributes nearly 50% of the net heat release. However at flow rates approaching quenching limits, $H + O_2(+M) \rightarrow HO_2(+M)$ is the elementary reaction with the largest heat release rate.

Keywords: Inverse flame; Kinetic extinction; Laminar flame; Microflame; Microgravity

1. Introduction

This study is motivated by the limited understanding of quenching limits of weak diffusion flames, particularly those fueled by hydrogen. Such quenching limits are pertinent to the fire hazards associated with small leaks in hydrogen systems and the potential use of microcombustors for power generation. They could also affect kinetic extinction phenomena in turbulent diffusion flames and fires, particularly those associated with flame anchoring and stability [1–3].

Quenching limits are defined as conditions for which a stable flame will extinguish upon any reduction in flow rate. These limits are associated with kinetic extinction, which occurs at high scalar dissipation rates (low Damköhler numbers) and may occur with or without external losses (i.e., losses other than chemical enthalpy loss). This is contrary to radiative extinction, which occurs at high Damköhler numbers and to date has only been conclusively observed in spherical diffusion flames in microgravity [4]. Spherical diffusion flames allow the investigation of both

* Corresponding author. Address: Dept. of Fire Protection Engineering, University of Maryland, 3104 J.M. Patterson Building, College Park, MD 20742, USA. Fax: +1 (301) 405 9383.
E-mail address: pbs@umd.edu (P.B. Sunderland).

1540-7489/$ - see front matter © 2012 The Combustion Institute. Published by Elsevier Inc. All rights reserved.
http://dx.doi.org/10.1016/j.proci.2012.07.029

kinetic and radiative extinction, at low and high flow rates, respectively.

Microcombustors have potential advantages over batteries in terms of power generation per unit volume and energy storage per unit mass [5]. Recent developments in microelectromechanical systems (MEMS) have enabled microcombustors with dimensions on the order of 1 mm [5]. Weak but stable flames are important to microcombustor design.

While there has been extensive research on normal microflames, i.e., flames with fuel issuing into an oxidizer, this is the first study to consider inverse microflames. Inverse flames involve the injection of oxidizer into surrounding fuel and can arise in, for example, turbulent flames, industrial processes, or under-ventilated fires.

Butler et al. [6] examined weak hydrogen flames that might be associated with the fire hazards of small hydrogen leaks. They observed quenching limits of diffusion flames on small round burners and found the quenching mass flow rates for hydrogen to be about an order of magnitude lower than those for methane and propane. At the quenching limits the flame height was comparable to the quenching distance for premixed hydrogen flames, in agreement with other studies [7,8]. Significantly smaller quenching limits for hydrogen were also observed for leaking compression fittings [6]. These hazards are now recognized in an SAE recommended practice [9].

Several studies have examined flames that are among the weakest ever observed. Ronney et al. [10] observed the burning of microgravity premixed flame balls during the STS-83 Space Shuttle mission, with heat release rates as low as 0.5–1 W. Weak propane flames anchored on a 0.1 mm tube were found to have heat release rates as low as 1 W [7], while methane diffusion flames as weak as 0.5 W were predicted numerically [8]. The weakest flames observed to date were fueled by hydrogen flowing downward into air and oxygen from a tube with an inside diameter of 0.15 mm [6,11]. These flames had heat release rates as low as 0.46 W in air and 0.25 W in oxygen.

Past work has found microflames in microgravity to resemble those in normal gravity. Methane gas jet diffusion flames on burners smaller than 1 mm were predicted to be nearly hemispherical for Peclet numbers less than 5 [8]. Small hydrocarbon jet flames were observed and predicted to be only slightly affected by buoyancy and to be nearly hemispherical [7,12]. Microjet hydrogen diffusion flames with hydrogen issuing from tubes of 0.2 and 0.48 mm were hemispherical near extinction [13].

To capture the fundamental nature of kinetic extinction associated with quenching limits in normal and inverse hydrogen flames, a one-dimensional spherical diffusion flame geometry is considered here. In addition to allowing the study of quenching in an unstretched, idealized diffusion flame, these flames are computationally attractive and allow for the study of convection direction independently from the flame stoichiometric mixture fraction, which is not possible, for example, in counterflow diffusion flames.

2. Numerical methods

The solver employed here was modified from PREMIX [14] to admit diffusion flames. Conservation of mass, species, and energy at steady state were solved in 1-D spherical geometry [4,15]. The flow was assumed to be isobaric and laminar. Conventional finite difference techniques with non-uniform mesh were adopted to discretize the conservation equations. The equations were solved using TWOPNT [16], which adopts a modified damped Newton's method to solve boundary value problems. The diffusive and convective terms were expressed by central and upwind difference formulas, respectively. Reaction rates, thermodynamic properties, and transport properties were evaluated using CHEMKIN and the TRANSPORT library [17,18]. A detailed H_2/air chemistry model was extracted from USC Mech Version II [19]. It comprises 9 species and 28 reactions. The hydrogen chemistry model from GRI-Mech 3.0 was also tested, and the results differed only slightly from those presented here.

A mixture-average formulation was adopted to compute species diffusivity coefficients. Diffusion due to temperature gradients (Soret diffusion) was included. Simulations using multicomponent diffusion did not significantly change the results, nor did the deactivation of Soret diffusion. Because the diffusion coefficients of H, H_2, and other light species are not well modeled by the Lennard-Jones potential function, their values were adjusted [20,21].

The burner surface was specified as adiabatic and nonradiating, and species fluxes, rather than concentrations, were specified there. This prevented the loss of heat or species into the burner from the surrounding gas and is similar to the approach of Santa et al. [4,15], and Mills and Matalon [22]. The outer boundary was a Dirichlet boundary with a temperature of 300 K and a composition of either air (for normal flames) or H_2 (for inverse flames). The outer boundary was located at a radius of 150 cm. Tests with a larger domain confirmed this was sufficient to be considered infinite.

Adaptive mesh point addition was used to ensure grid independence. Low tolerances were used to refine the mesh. Radiative heat loss from the gases was neglected because this is small for hydrogen flames near their kinetic extinction limits [23], particularly for microflames [24]. Because this study focused on kinetic extinction without

heat loss, surface radiation was also neglected. Radiative loss from the burner surface is small for flames that are detached from the burner, but might become significant for flames that are anchored to the burner [23].

Local mixture fraction is defined following Bilger [25] as:

$$Z = \frac{\frac{Y_H}{M_H} + \frac{2(Y_{O,ox} - Y_O)}{M_O}}{\frac{1}{M_H} + \frac{2Y_{O,ox}}{M_O}}, \quad (1)$$

where Y is the local mass fraction, M is atomic mass, the subscripts denote the element considered, and ox is the oxidizer supply. Local equivalence ratio is defined as:

$$\varphi = (Z - 1)/(Z_{st} - 1), \quad (2)$$

where the subscript st denotes stoichiometric conditions, i.e., conditions for the present H_2/air flames with $Z_{st} = 0.0283$. Local scalar dissipation rate is defined as:

$$\chi = 2\alpha(dZ/dr)^2, \quad (3)$$

where α is mixture thermal diffusivity and r is radius.

In identifying quenching limits, a steady flame solution was used as the starting condition for a new simulation at a decreased mass flow rate. Extinction was identified when a solution showed no temperature increase above ambient.

3. Results

Before examining quenching limits, larger normal and inverse flames are considered in Figs. 1 and 2, respectively. Similar to the approach of Sunderland et al. [26], these flames have matched total heat release rates and H_2 consumption rates under the assumption of complete combustion. For a normal flame with a fuel flow rate well above its quenching limit, Fig. 1a shows the predicted structure. (Herein structure is defined as the variation of temperature and mole fraction with respect to position or mixture fraction.) This flame has hydrogen issuing at 10 mg/s from a 5 mm radius burner, although a reduced burner size has no significant effect on the predictions. Figure 1a depicts a flame with the structure of a canonical diffusion flame. The temperature, T, peaks at 2305 K (which is close to the adiabatic flame temperature) and the overall heat release rate is 1286 W.

Figure 1b shows the net heat release, Q_{net}, and the heat release rates Q associated with the main heat releasing reactions. There are two peaks of Q_{net}. Both peaks are dominated by $H + OH(+M) \rightarrow H_2O(+M)$. The flame has two main endothermic reactions, $H + O_2 \rightarrow O + OH$ and the reverse of $2OH \rightarrow O + H_2O$. The latter arises from the high concentrations of H_2O near

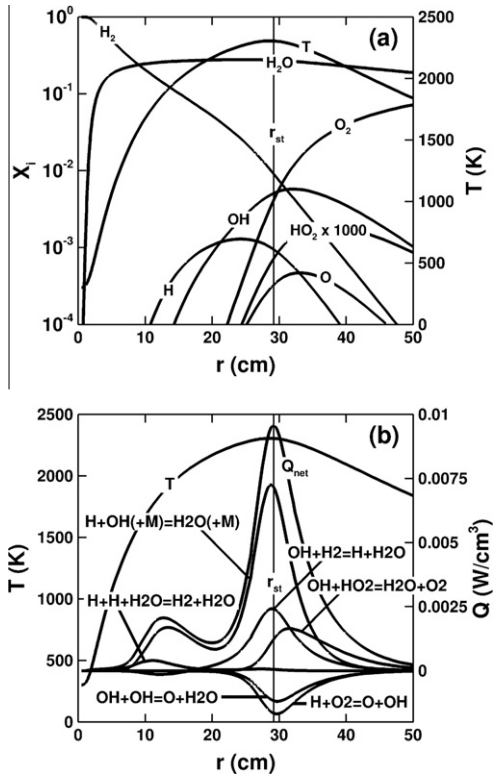

Fig. 1. Flame structure (a) and local heat release rates (b) for a large H_2/air normal flame on a 5 mm radius burner. Hydrogen flow rate and χ_{st} are 10 mg/s and $3.8 \times 10^{-6}\,s^{-1}$.

r_{st}. The low χ_{st} ($3.8 \times 10^{-6}\,s^{-1}$) results in a broad reaction zone that spans a 50 cm radius. The reaction zone is bounded between the two locations where $Q_{net}/Q_{net,peak} = 0.01$.

Figure 2 presents the predicted structure and heat release rates associated with the main heat releasing reactions for an inverse flame with an oxidizer flow rate well above the quenching limit. This flame has air issuing at 340 mg/s from a 5 mm radius burner. Like the flame of Fig. 1, this flame has the structure of a canonical diffusion flame. The overall heat release rate is 1253 W, which is similar to the flame of Fig. 1, but the flame is smaller (based on r_{flame}) and has a narrower reaction zone that spans only 3.2 cm of radius. Independence of the results on the burner size was again confirmed.

There are several differences in structure and chemistry between the flames of Figs. 1 and 2. The peak temperature of the inverse flame, 2596 K, is 290 K higher than that of the normal flame. This arises because the Lewis number (defined as the mixture thermal diffusivity divided by the reactant mass diffusivity) of the ambient reactant in the inverse flame (H_2) is much lower

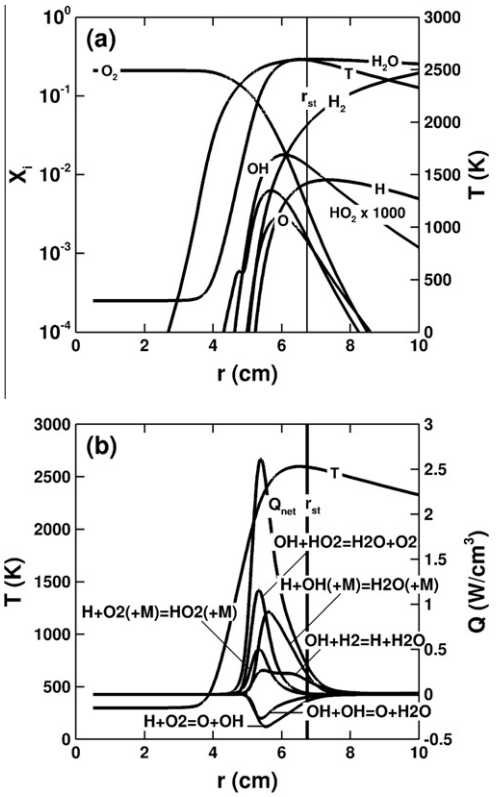

Fig. 2. Flame structure (a) and local heat release rates (b) for a large H_2/air inverse flame on a 5 mm radius burner. Air flow rate and χ_{st} are 340 mg/s and 9.4×10^{-4} s^{-1}.

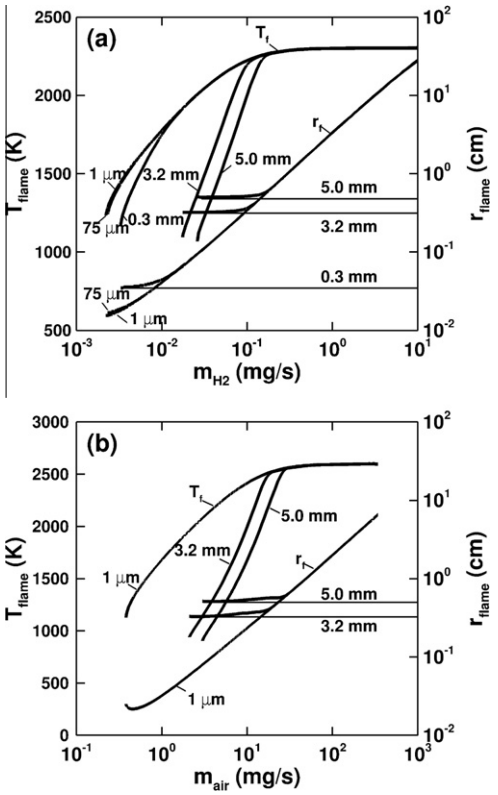

Fig. 3. Predicted H_2/air peak temperature and its radius for various burner radii versus (a) hydrogen flow rate for normal flames and (b) air flow rate for inverse flames.

than unity, whereas for the normal flame it is nearly unity. This is in agreement with asymptotic analyses of steady-state spherical diffusion flames, which also predict an increase (albeit smaller) in peak temperature with decreasing Lewis number [22]. In addition, the inverse flame has a peak temperature that is slightly on the lean side of stoichiometric and has higher radical mole fractions. Only a single peak of Q_{net} is observed in the inverse flame, which is on the lean side of stoichiometric owing to the low ambient Lewis number. The main exothermic reactions are $H + OH(+M) \rightarrow H_2O(+M)$ and $OH + HO_2 \rightarrow H_2O + O_2$, while the main endothermic reactions are $H + O_2 \rightarrow O + OH$ and the reverse of $2OH \rightarrow O + H_2O$.

Simulations for various burner sizes and flow rates were performed. Figure 3a and b shows the variation of peak temperature, T_{flame}, and its radius, r_{flame}, for normal and inverse flames, respectively. The highest flow rates correspond to the flames of Figs. 1 and 2. For flow rates above 0.2 mg/s (normal flames) or 3 mg/s (inverse flames), T_{flame} remains close to its asymptotic value, burner radius has no significant effect on T_{flame} or r_{flame}, and r_{flame} increases with burner mass flow rate according to:

$$r_{flame} \sim \dot{m}^{0.95}. \quad (4)$$

This is close to theoretical predictions of $r_{flame} \sim \dot{m}$ for quasi-steady burning of spherical droplets [27] and porous-burner flames [22,23,28].

Flames approaching their quenching limits behave quite differently. For flames with burners larger than 1 μm, r_{flame} ultimately reaches the burner surface, while T_{flame} decreases. A departure from linearity between flow rate and flame radius occurs at small flow rates. This is similar to behavior predicted by Fursenko et al. [28] for flames with significant heat losses to the burner. The underlying mechanisms are different in the present work because there is no heat loss to the burner. Owing to the collapse of the flame onto the burner, significant ambient air in the reaction region of normal flames (or ambient hydrogen in the reaction region of inverse flames) results in transition to the premixed-flame regime of diffusion flames, as will be discussed in more detail later. The peak temperature at the quenching limits

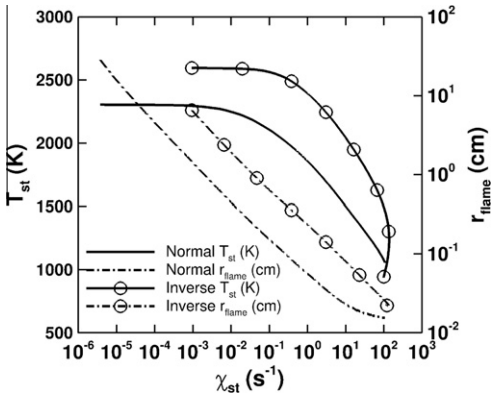

Fig. 4. Predicted H_2/air temperature at stoichiometry and flame radius versus stoichiometric scalar dissipation rate for normal and inverse flames for a 1 μm radius burner.

decreases with burner size and is higher for normal flames (1070–1240 K) than for inverse flames (903–1127 K).

It is only for a burner radius as small as 1 μm that the flames do not collapse onto the burner when approaching the quenching limit. While such small spherical burners cannot be fabricated, they are modeled here to examine microflame structure without burner interference. For the 1 μm radius burner, T_{flame} is a strong function of flow rate near the quenching limit. The hydrogen flow rate at the quenching limit is 2.2 μg/s for the normal flame, corresponding to a heat release rate of 0.24 W. The entire flow field is lean, with an equivalence ratio at peak temperature of 0.51. Note that a normal flame of hydrogen burning downward in air on a 0.15 mm tube was observed to have a quenching limit of 3.9 μg/s and 0.46 W [6,11]. The reasonable agreement between measured and predicted quenching limits lends support to past claims that microflames in normal gravity are nearly nonbuoyant and hemispherical [7,8,12,13]. The air flow rate at the quenching limit is 0.38 mg/s for the inverse flame, corresponding to a heat release rate of 1.38 W. The entire flow field is rich, with an equivalence ratio at peak temperature of 2.75.

As flow rate decreases, r_{flame} and T_{flame} generally decrease (see Fig. 3), while χ_{st} increases. Mills and Matalon [22] considered adiabatic spherical diffusion flames and found that the Damköhler number, D_a, scales with $\dot{m}^2$. In spherical flames, decreasing the mass flow rate decreases the transport time until it is comparable to the chemical time near quenching conditions [29]. A representation of transport times is χ_{st}^{-1}, such that:

$$D_a \sim \chi_{st}^{-1} \exp(-E_a/R_u T_{st}), \tag{5}$$

where E_a is the activation energy and R_u the universal gas constant. Comparing Eq. (5) with results of Ref. [22] yields $\chi_{st} \sim \dot{m}^{-2}$ such that a decrease in $\dot{m}$ leads to a sharp increase in χ_{st}.

Figure 4 plots T_{st} and r_{flame} versus χ_{st} for the normal and inverse flames for a burner radius of

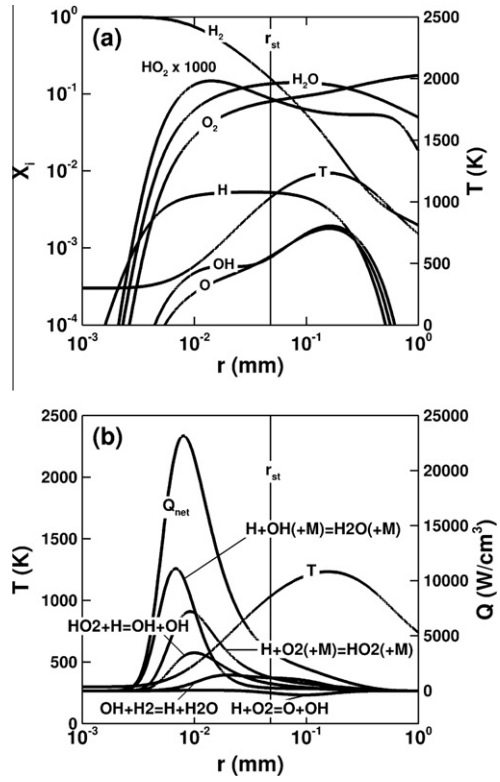

Fig. 5. Species mole fractions (a) and selected local heat release rates (b) for the weakest normal flame on a 1 μm radius burner. Hydrogen flow rate and χ_{st} are 2.23 μg/s and 107 s^{-1}.

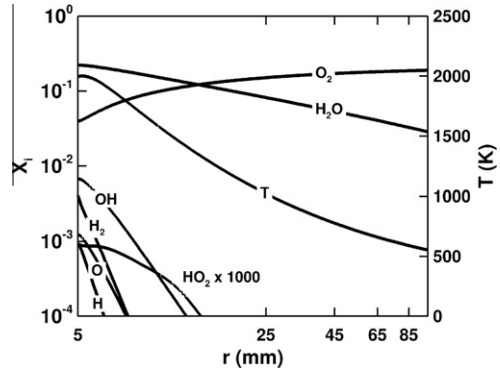

Fig. 6. Species mass fractions and temperature for a H_2/air normal flame that has collapsed onto the 5 mm radius burner. Hydrogen flow rate and χ_f are 0.1 mg/s and 0.022 s^{-1}.

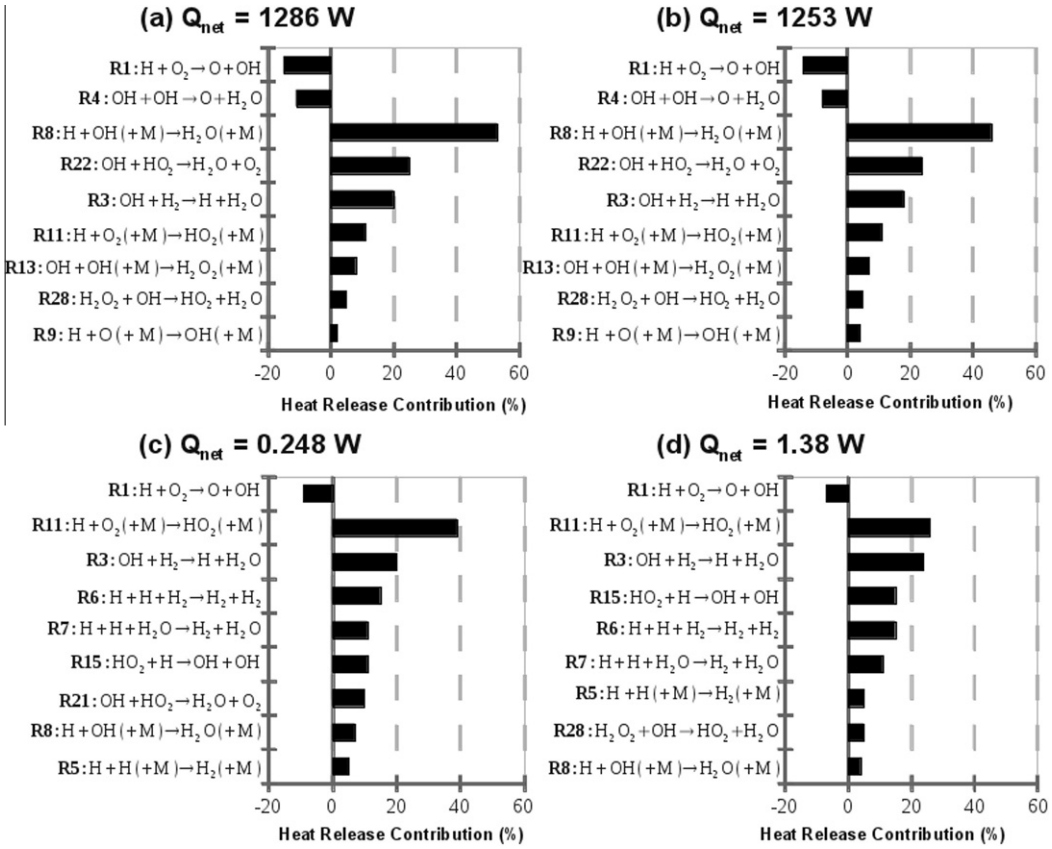

Fig. 7. Normal (a, c) and inverse (b, d) flame key endothermic and exothermic reactions. Plots (c) and (d) are near quenching.

1 μm. Inverse flames have higher peak temperatures than normal flames over a broad range of scalar dissipation rate. While inverse flames are smaller than normal flames at matched heat release rates, Fig. 4 shows that inverse flames are larger at matched scalar dissipation rates. For both configurations, at low values of χ_{st} (i.e., high $\dot{m}$) T_{st} is independent of χ_{st}. A decrease of $\dot{m}$ leads to an increase in χ_{st}. This in turn yields a reduction in T_{st} owing to chemical enthalpy loss via burner reactant leakage across the reaction zone into the ambient. The high values of χ_{st} at quenching, 107 and 98 s^{-1} for the normal and inverse flame, respectively, confirm that the quenching limits are kinetic extinction events.

Figure 5a shows the structure of a normal flame near quenching on a 1 μm radius burner. Its peak temperature is 1252 K and is located 155 μm from the origin. This flame has a high peak HO_2 mole fraction, about 100 times that of the larger normal flame of Fig. 1. Extensive reactant leakage occurs. This is still a canonical diffusion flame owing to the small size of the burner, with pure hydrogen present at the burner surface. Figure 5b shows the local total heat release rate and the main heat release reactions for this flame. High heat release rate densities are observed, up to 20 kW/cm^3. The main reactions in terms of heat released are: $H + OH(+M) \rightarrow H_2O(+M)$; $H + O_2(+M) \rightarrow HO_2(+M)$; $HO_2 + H \rightarrow 2OH$ (which corresponds to the 3rd explosion limit reaction); $OH + H_2 \rightarrow H + H_2O$; and $H+O_2 \rightarrow O + OH$.

It is of interest to consider a flame that collapses onto the burner prior to quenching. One such flame is shown in Fig. 6, which is a normal flame on a 5 mm radius burner with 100 μg/s of hydrogen flowing. The peak temperature radius is 5.18 mm and abundant O_2 is present at this location. Radical levels at the burner surface are comparable to those predicted for the larger flame of Fig. 1. Despite considerable reactant leakage, radical mole fractions have not been reduced.

Figure 6 demonstrates the existence of a premixed flame regime in a diffusion flame, as introduced by Liñán [30]. For the flames studied in this work this regime occurs when significant ambient reactant leaks through the reaction zone and reaches the burner. The reaction rate becomes controlled by the deficient reactant (here this is the

reactant supplied from the burner). In this regime, one of the reactants has a mass fraction of order unity in the entire reaction zone, as illustrated in Fig. 6. This is different from the diffusion flames of Buckmaster and Ludford [29] and Cheatham and Matalon [31], where minimal reactant leakage across the reaction zone is allowed. No diffusion flame burning steadily in the premixed flame regime has been observed before because this is in the physically unrealistic middle branch of the S curve and thus requires unusual conditions such as those present here. The deviation from the typical diffusion flame structure, e.g., that in Fig. 1, indicates the transition to the premixed flame regime (instead of extinction) when the mass flow rate is reduced and the flame becomes attached to the burner. Extinction in this flame is similar to that in lean premixed flames and occurs at a hydrogen flow of 26 μg/s and a peak temperature of 1070 K.

Figure 7 shows the key reactions and their fractional contributions to overall heat release rate for: (a) the normal flame of Fig. 1; (b) the inverse flame of Fig. 2; (c) the normal flame of Fig. 5; and (d) an inverse flame near quenching. Negative quantities denote endothermic reactions. Far from quenching, normal and inverse flames (Fig. 7a and c) have the same key reactions. The main heat producer is $H + OH(+M) \rightarrow H_2O(+M)$, yielding nearly 50% of the overall heat release. However, $OH + H_2 \rightarrow H + H_2O$ has the highest rate of progress. The HO_2 producing reactions account for only 15% of the heat produced. Near the quenching limits, the key reactions are different as summarized in Fig. 7c and d for normal and inverse flames, respectively. Here there is only one key endothermic reaction, $H + O_2 \rightarrow O + OH$. The main heat producing reaction is $H + O_2(+M) \rightarrow HO_2(+M)$, which accounts for 40% and 25% of the overall heat release for normal and inverse flames, respectively. The reaction $OH + H_2 \rightarrow H + H_2O$ is the second most important reaction for both flames. For the larger flames $OH + H_2 \rightarrow H + H_2O$ has the highest rate of progress. The recombination of H_2 accounts for more than 30% of the overall heat release in both normal and inverse flames.

4. Conclusions

Quenching limits of hydrogen/air spherical diffusion flames were investigated for normal and inverse configurations. The burners were adiabatic porous spheres of various sizes. The flames were simulated using a steady-state laminar flame code with detailed chemistry and transport. The main conclusions are as follows.

1. At equivalent heat release rates, inverse flames are smaller and hotter than normal flames. For large flow rates, the peak temperature of normal flames is the adiabatic flame temperature, while that of inverse flames is 290 K hotter. This difference results from the low Lewis number of the ambient gas for inverse flames fueled by hydrogen.
2. There is extensive reactant leakage for conditions approaching extinction. Flames supported by burners on the order of 1 μm in radius do not collapse onto the burner prior to quenching. Such collapse does occur for larger burners, leading here to the first demonstration of the premixed flame regime of diffusion flames, as introduced by Liñán.
3. Lower quenching limits are predicted for normal flames, with a lower bound of 0.25 W. This is similar to quenching limits measured in normal gravity on tube burners. Inverse flames quench at a heat release rate as low as 1.38 W. The minimum peak temperatures at the quenching limits are 1070 and 903 K for normal and inverse flames, respectively.
4. For large flames the spatially resolved heat release rate has either a double peak (normal flames) or a single peak (inverse flames). For these flames $H + OH(+M) \rightarrow H_2O(+M)$ is the main heat producing reaction. Flames closer to quenching have a single peak in heat release rate and have $H + O_2(+M) \rightarrow HO_2(+M)$ as the main heat producing reaction.

Acknowledgments

This work was funded by NASA (D.P. Stocker, grant monitor) and by NIST (J. Yang, grant monitor).

References

[1] R. Chen, R.L. Axelbaum, *Combust. Flame* 142 (2005) 62–71.
[2] H.Y. Wang, W.H. Chen, C.K. Law, *Combust. Flame* 148 (2007) 100–116.
[3] F.A. Williams, *Fire Safety J.* 3 (1981) 163–175.
[4] K.J. Santa, B.H. Chao, P.B. Sunderland, D.L. Urban, D.P. Stocker, R.L. Axelbaum, *Combust. Flame* 151 (2007) 665–675.
[5] A.C. Fernandez-Pello, *Proc. Combust. Inst.* 29 (2002) 883–899.
[6] M.S. Butler, C.W. Moran, P.B. Sunderland, R.L. Axelbaum, *Int. J. Hydrogen Energy* 34 (2009) 5174–5182.
[7] L.M. Matta, Y. Neumeier, B. Lemon, B.T. Zinn, *Proc. Combust. Inst.* 29 (2002) 933–939.
[8] Y. Nakamura, H. Yamashita, K. Saito, *Combust. Theory Model.* 10 (2006) 927–938.
[9] SAEJ2579, *Recommended Practice for General Fuel Cell Vehicle Safety, A Surface Vehicle Recom-*

mended Practice, SAE International, Detroit, MI, 2009.
[10] P.D. Ronney, M.S. Wu, H.G. Pearlman, K.J. Weiland, *AIAA J.* 36 (1998) 1361–1368.
[11] V.R. Lecoustre, P.B. Sunderland, B.H. Chao, R.L. Axelbaum, *Combust. Flame* 157 (2010) 2209–2210.
[12] H. Han, S. Venkatesh, K. Saito, *J. Heat Transfer* 116 (1994) 954–959.
[13] T.S. Cheng, Y.C. Chao, C.Y. Wu, Y.H. Li, Y. Nakamura, K.Y. Lee, T. Yuan, T.S. Leu, *Proc. Combust. Inst.* 30 (2005) 2489–2497.
[14] R.J. Kee, J.F. Grcar, M.D. Smooke, J.A. Miller, E. Meeks, *Premix: A FORTRAN Program for Modeling Steady Laminar One-Dimensional Premixed Flames*, Report No. SAND85-8240, Sandia National Laboratories, 1987.
[15] K.J. Santa, Z. Sun, B.H. Chao, P.B. Sunderland, R.L. Axelbaum, D.L. Urban, D.P. Stocker, *Combust. Theory Model.* 11 (2007) 639–652.
[16] J.F. Grcar, *The Twopnt Program for Boundary Value Problems*, Report No. SAND91-8230, Sandia National Laboratories, 1991.
[17] R.J. Kee, F.M. Rupley, E. Meeks, J.A. Miller, *Chemkin-III: A Fortran Chemical Kinetics Package for the Analysis of Gas-Phase Chemical and Plasma Kinetics*, Report No. SAND96-8216, Sandia National Laboratories, 1996.
[18] R.J. Kee, G. Dixon-Lewis, J. Warnatz, M.E. Coltrin, J.A. Miller, H.K. Moffat, *A Fortran Computer Code Package for the Evaluation of Gas-Phase Multicomponent Transport Properties*, Report No. SAND86-8246, Sandia National Laboratories, 1988.
[19] H. Wang, X. You, A.V. Joshi, S.G. Davis, A. Laskin, F. Egolfopoulos, C.K. Law, *USC Mech Version II. High-Temperature Combustion Reaction Model of H2/CO/C1–C4 Compounds,* 2007, available at http://ignis.usc.edu/USC_Mech_II.htm.
[20] H. Wang, *Chem. Phys. Lett.* 325 (2000) 661–667.
[21] P. Middha, B. Yang, H. Wang, *Proc. Combust. Inst.* 29 (2002) 1361–1369.
[22] K. Mills, M. Matalon, *Combust. Sci. Technol.* 129 (1997) 295–319.
[23] Q. Wang, B.H. Chao, *Combust. Flame* 158 (2011) 1532–1541.
[24] T.S. Cheng, C.Y. Wu, C.P. Chen, Y.H. Li, Y.C. Chao, T. Yuan, T.S. Leu, *Combust. Flame* 146 (2006) 268–282.
[25] R.W. Bilger, *Proc. Combust. Inst.* 22 (1988) 475–488.
[26] P.B. Sunderland, R.L. Axelbaum, D.L. Urban, B.H. Chao, S. Liu, *Combust. Flame* 132 (2003) 25–33.
[27] C.K. Law, *Combust. Flame* 24 (1975) 89–98.
[28] R.V. Fursenko, S.S. Minaev, K.C. Chang, Y.C. Chao, *Combust. Expl. Shock Waves* 44 (2008) 1–8.
[29] J. Buckmaster, G.S.S. Ludford, *Lectures on Mathematical Combustion*, The Universities Press, Belfast, 1983 (Chapter 9).
[30] A. Liñán, *Acta Astronaut.* 1 (1974) 1007–1039.
[31] S. Cheatham, M. Matalon, *J. Fluid Mech.* 414 (2000) 105–144.